A Novel High Capacity Space Efficient Heat Storage system for Domestic Applications

Elamin Awad Mohamed*[1], Siddig Omer, Saffa Riffat

The University of Nottingham, UK

Author*[1]: Amin_eissawi@alumni.nottingahm.ac.uk

Abstract

Energy consumption in domestic buildings is dominated by space heating 60 percent followed by hot water 14 percent in the UK. Space heating and water heating confers a disparate set of industrial challenges to the manufacture and this is a very demanding objective, which necessitates novelty. Space heating and water heating functions will become more significant as the trend towards low energy homes rises for a fully integrated system. The most common practical heat storage's are water and latent heat of fusion storage media. The new Thermochemical reaction materials regarded as most promising materials for the ability of store sufficient heat for practical domestic requirements. The volume capacities of materials play a key role for choosing storage system and this have a direct bearing on the performance of the heat storage system for domestic heating and heating water. Innovative thermal energy storage was conducted in a new concept for domestic applications at the Laboratory University of Nottingham, UK. An initial result has been investigated experimentally

Keywords: Solar Energy, Heat pump, Heat storage, Thermochemical reaction materials, heating system applications

Nomenclature

$COP_{h\text{-}sys}$ (t)	Heat pump coefficient of performance (air)
$COP_{h\text{-}sys,\ av}$	Coefficient of performance average of the system (air)
$COP_{w\text{-}sys}$ (t)	Heat pump coefficient of performance (water)
$COP_{w\text{-}sys,\ av}$	Coefficient of performance average of the system (water)
$COP_{effective}$	Coefficient of performance effectiveness of the system
$Q_h(t)$	Heat exchange rate in the plate condenser, W
Q_w (t)	Condenser gained heat delivered by heat pump (water), W
$W\ (t)$	System input power, W
$Q_{evaporate}$	Evaporator heat gained experimentally, W
$Q_{condenser_{air}}$	Condenser heat gained experimentally, W
U_L	Collector heat losses, W/m²/deg
h_w	Wind heat transfer coefficient, $W*m^{-2}$
Q_{Solar}	Collector heat gained theoretically, W
m_r	Refrigerant mass flow rate, $kg*s^{-1}$
F'	Collector efficiency factor
F	Fin efficiency factor of the collector plate
D	Refrigerant tube diameter, m
D_i	Inside refrigerant tube diameter, m
hf_i	Heat transfer coefficient
R_e	Reynold number
P_r	Prandtl number
T_a	Ambient temperature, °C
T_2	Outlet collector's temperature, °C
T_3	Discharge compressor temperature, °C
$\check{T}$	Mean refrigerant temperature in the collector/evaporator, °C
V	Compressor velocity, rpm
$\dot{m}_{coll\_ref}$	Refrigerant mass flow rate, $kg*s^{-1}$
η_{coll_ref}	Collector efficiency, %
N_u	Nusselt number
Ac	Area of solar collector, m²
W_{comp}	Compressor work, W
η_{comp}	Compressor efficiency, %
SPF	Seasonal performance factors
ρ	Fluid density ($k_g * m^{-3}$)
h_{refout}	Refrigerant/Collector outlet enthalpy ($kJ*kg^{-1}$)
h_{refin}	Refrigerant/ Collector inlet enthalpy ($kJ*kg^{-1}$)
$\propto$	Collector adsorption rate
A_t	Total heat transfer area of the wall of the water tank, m
τ	Operating period of duration, per-minutes
$U_{L,t}$	Water condenser heat losses, W/m²/deg
C_{pw}	Water specific heat
M_w	Water mass in the water tank
I_{coll}	The intensity of the solar radiation in ($W*m^{-2}$)
Inlet air, av	Average of outdoor air temperature, °C
T_{room}	Room temperature, °C
HR, av	Average of hot air rejected by condenser, °C

1. Introduction

Among the available energy resources, solar energy is considered readily available, cheap and non-polluting which can be used in industrial or domestic low temperature thermal applications. Solar energy systems and heat pumps are one of the promising means of decreasing the consumption of fossil fuel. The idea of powering heat pumps with solar energy has been investigated and proposed by many researchers around the world, and is related to solar-assisted heat pump (SAHP) system. Numerical and experimental studies on the performance of SAHP systems were implemented as early as in the 1970s (Freeman, Mitchell et al. 1979) and the theoretical and experimental SAHP studies were performed in the 1990s (Ito, Miura et al. 1999). Huang and Chyng (1999) first suggested the design of an integral-type solar-assisted heat pump (DX-SAHP) that integrates the heat pump, solar collector, to come up with a single unit that is easy to install. (Kuang, Sumathy et al. 2003) has performed experimental and analytical studies on direct-expansion solar-assisted heat pump (DX-SAHP) as applied in Shanghai. The effects of various parameters under constant compressor speed were investigated.

A further developed DX-SAHP system which was able to supply multi-functional low heating costs to domestic buildings, including space cooling during the summer, space heating during the winter, and hot water supply for the whole year was investigated by (Kuang and Wang 2006). Despite of the above-mentioned advantages the use of heat pump for combined space heating and water heating, particularly the solar-assisted heat pump (DX-SAHP) options, is not popular. The above studies, however, did not investigate the energy performance of DX-SAHP for both water and the space heating using one unit. A multi-fold-functional system in the cold climate region is essential throughout the year and high utilization rate makes the option economically attractive(Chow, Pei et al. 2010). Moreover, the coefficient of performance of the (DX-SAHP) system would increase over that of the air-source heat pump system alone(Kong, Zhang et al. 2011). DX-SAHP can utilize heat from solar radiation and ambient air simultaneously (Huang and Chyng 2001), and can also operate using surrounding domestic-industrial exhausted heating. Even in the absence of solar insulation, this can be used for space heating and water heating applications. On the other hand to increase the evaporation temperature, unglazed solar collectors can be used by acting as an evaporator to increase the thermal performance of the heat pump.
Various types of collectors have been considered but a unique fabricated design of collectors in heat pump systems have been built and investigated. This paper presents an analysis of a solar assisted heat pump space heating and water heating system in which unglazed flat plate collectors act as an evaporator for the heat pump. Refrigerant 407c is used as a working fluid. Analytical and experimental investigations have been carried out and the analytical results are compared with those obtained from experimental results under various conditions. The influence of various operating parameters have been examined and the important variables that impact the performance are identified

The domestic sector in the UK currently accounts for ≈ 30% of national energy consumption and ≈ 25% of greenhouse gas emissions. This is because of the dependency on fossil fuels in domestic activities such as space and water heating. The UK government has identified micro generation as a key option for reducing greenhouse gas emissions from the domestic sector and for contributing towards UK's GHG reduction targets of 34% by 2020 and 80% by 2050.

In the UK micro generation is defined as the generation of electricity of up to 50 kW and or heat of up to 45 kW from a low carbon resource (Greening and Azapagic 2014).

Solar thermal micro generation systems could help reduce UK GHG emissions arising from solar and water heating in the domestic sector. Solar thermal is one of the most established micro generation technologies in the UK with more than 100 K units installed to date (Greening and Azapagic 2014). However this is still significantly lower compared to some countries such as Germany which has over 1 million units in operation. At this point thermal energy storage (TES) systems, integrated to solar thermal systems would have significant importance for the UK to increase their solar fraction and render solar thermal systems sustainable with low cost applications.

In this context, SHS and LHS systems have been widely researched and utilized in real applications for solar thermal energy storage. Thermochemical heat storage (THS) systems have gained attention in the last decade due to their higher heat storage density / lower volume requirement also long term heat storage potential without heat losses. This important aspect represents significant opportunities including inter-seasonal storage of solar energy, conversion and thermal storage of excess renewable energy sourced electricity (e.g photovoltaic panels), capturing / storing the industrial waste heat and utilizing off -peak electricity tariff with THS materials.

Majority of the work on low temperature THS has been focused on sorption material development and space heating applications. Investigations on THS systems in water heating applications are very limited in the literature. To fulfil this gap this paper presents a novel design integrating solar assisted heat pump and a hot water tank surrounded with a sorption jacket. The aim was to utilize off-peak electricity and/or electricity generated by PV panels to charge the sorption material. Charged sorption jacket, later slowly releases the stored heat while acting as insulation layer. This condition could minimizes the heat losses and reduce the energy consumption of heat pump to keep the water at desired temperature level, thereby provides a sustainable solution system to domestic water heating and space heating applications.

2. System description

A multi-mode-functional domestic DX-SAHP system is shown as Fig. 1. It mainly consists of a ternary unique coated aluminium flat-plate panel, a variable speed hermetic compressor, centrifugal

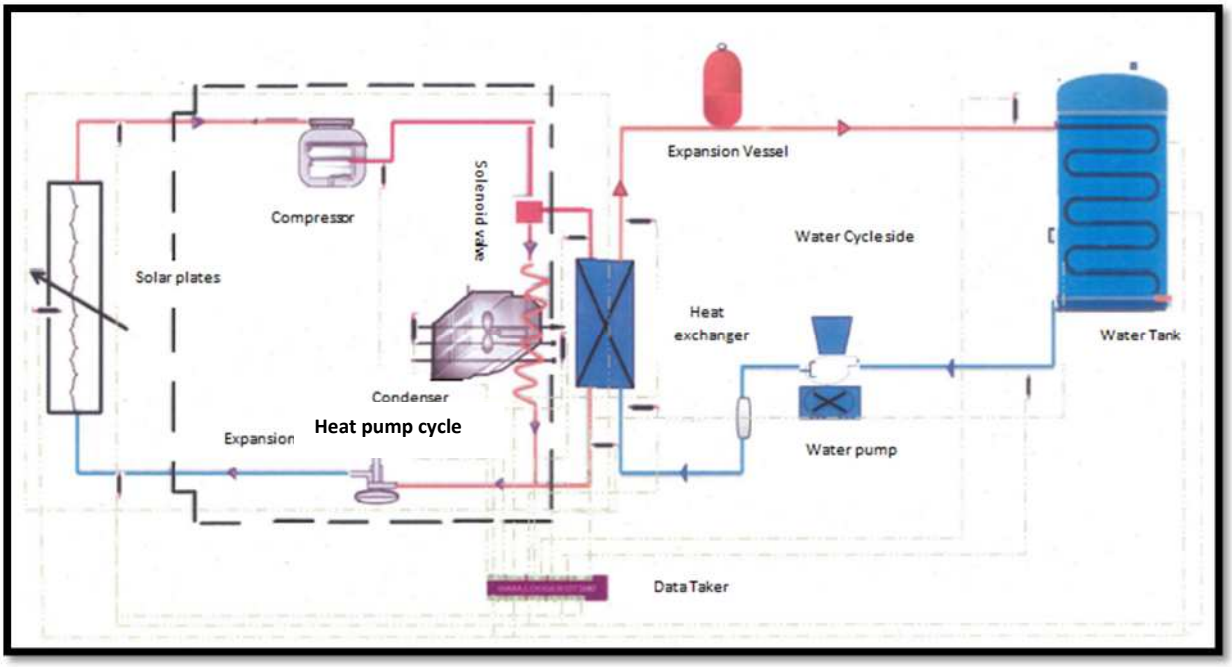

Figure 1: Schematic diagram of DX-SAHP multi-mode-functional system

fan -coil units (air-heat-exchanger), a water-to-refrigerant heat exchanger, a water circulating pump and piping, a hot water tank with an immersed condensing coil loop, thermostatic expansion valve and electrical valves.

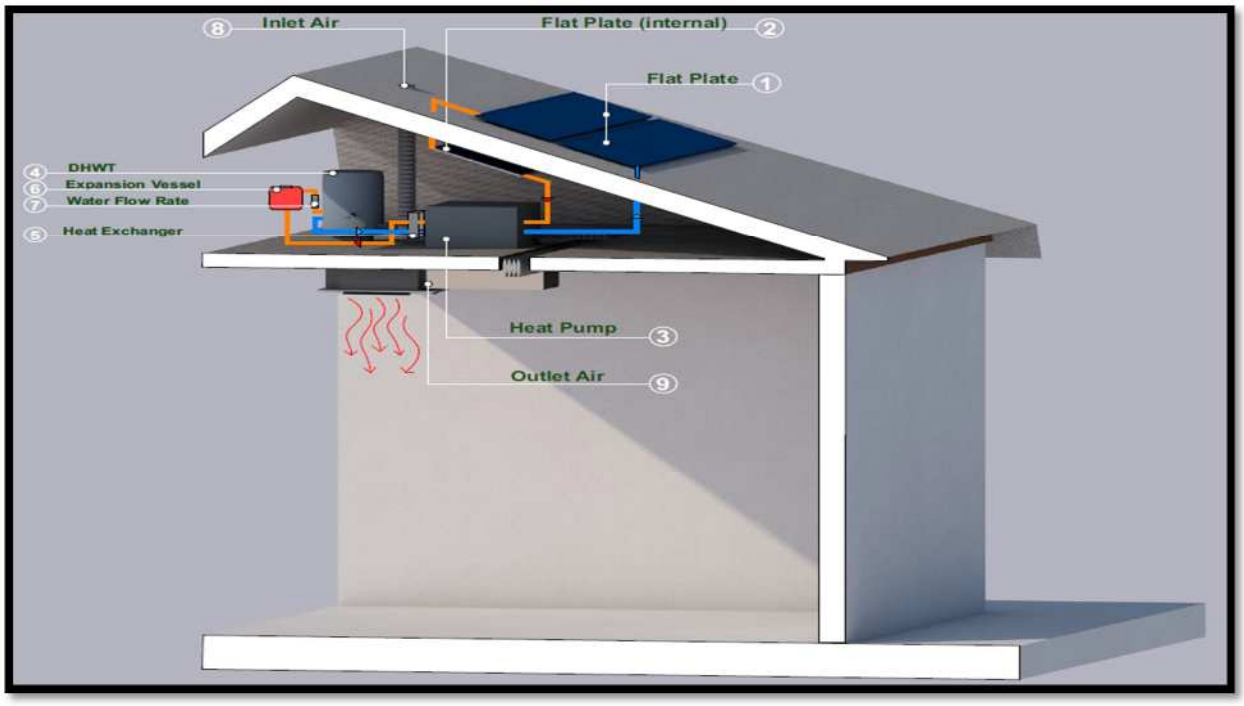

Figure 2: The system configurations on building's roof

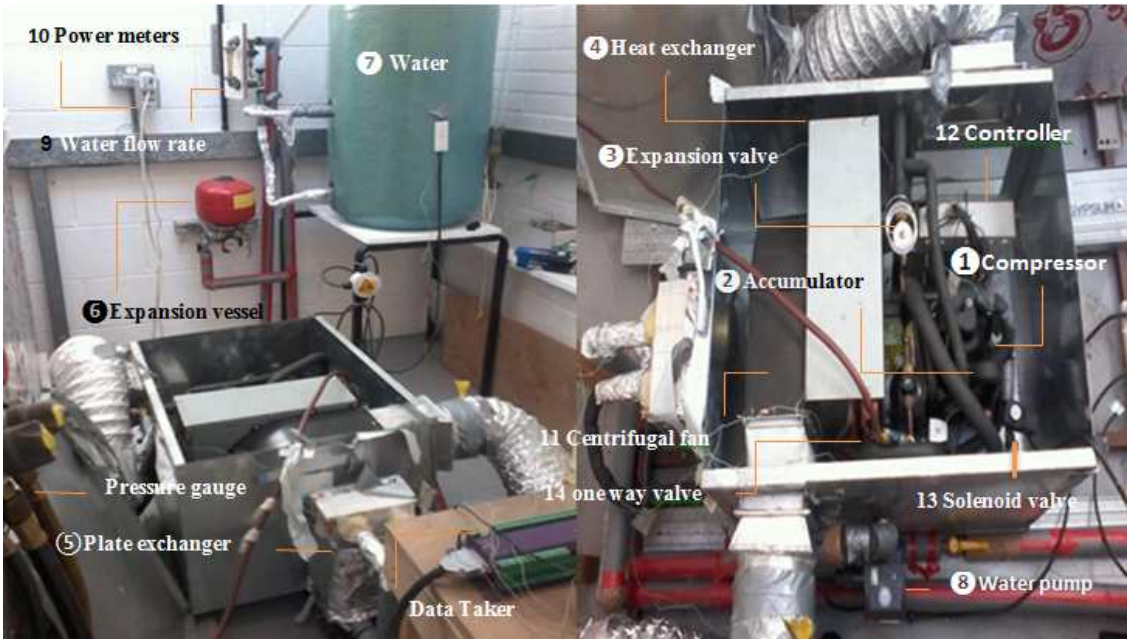

Figure 3: Experimental setup and components

The designed and fabricated un-glazed solar flat-plate collector was used as a heat source acting as an evaporator for the refrigerant R-407C. This unglazed solar absorber evaporator is formed by integrating bare ternary soft aluminium solar-collectors which were connected in series form **Fig.2**. The aluminium tubes are inlaid in the sheet, which were painted by a cover of black coating. Plate's thicknesses are 2mm while the diameter and thickness of aluminium tubes are 13mm and 2mm respectively. The collectors consist of two flat plates which are externally placed and integrated into the structure of a house roof, whereas another plate is internally mounted in the house loft space to absorb domestic wasted heat **Fig.2 (1, 2)**. The total surface area is 4.22 m^2. The Working fluid is disseminated inside the evaporator to absorb the solar energy. By a proper design of the refrigeration cycle and the collector for a specific operating condition, heat may be absorbed at low temperature, rather than rejected to the ambient. A direct expansion solar assisted heat pump (DX-SAHP) refrigeration cycle operates under quasi-static conditions during the UK winter season**Fig.2 (3)**. A hermetic-type compressor with a rated power of 800 W (50 Hz) was used in the system, with the compressor volumetric displacement of 7.84E-04 m^3/s.

The variation of the compressor's speed was obtained via variable frequency drive, to avert the compatibility between its variable loads in order to reach the steady capacity of the compressor **Fig.3 [1]**. A refrigerant receiver **Fig.3 [2]** and accumulator were included in the system to facilitate in controlling the refrigerant distribution, while the external pressure equalizer with thermal expansion valve controls the refrigerant's flow to the evaporators **Fig.3 [3]**, in order to attain constant superheat at the compressor inlet. The heat pump has two heat rejection modes, one of which is made of copper tube and aluminium fins**Fig.3 [4]**; to centrifuge energy to contribute for space-heating load in winter.

The other is copper tube as coil closed loop immersed in a 200 litre hot water tank, and water-to-refrigerant plate heat exchanger**Fig.3 [5]**. The water-to-refrigerant plate heat exchanger was linked to the hot water tank through circulating piping pump, expansion vessel **Fig.3 [6]** and water flow rate controller for hot water demands **Fig.3 [9]**. The energy rejected by condenser contributed to space-heating load in winter; whereas the storage tank is made of copper sheets fully insulated with a capacity of 200 litre **Fig.3 [7].**

3. Data acquisition and processing system

The temperatures, pressures and flow rate of R407C and water were measured at different locations in the system. Also, the ambient temperature, the incident solar insulation, and the collector surface, inlet/outlet, evaporation temperature were monitored **Fig.3 [16]**. Pressures were measured using pressure gages**Fig.3 [15]**. Temperatures were measured with constantan thermocouples and platinum resistance thermometers (RTDs) **Fig.3 [16]**. A solar pyranometer was used to maintain consistent solar radiation to cover the entire surface area of the plates equally. A flow meter was used to measure the water flow rate. Electronic power meters were utilised to measure the compressor's energy consumptions, and the power of the whole system including, pumps, electrical valves and fans, consecutively**Fig.3 [10]**. Thermal digital camera was chosen to display and analyse the temperature of components surfaces and its variations accurately and collecting relevant data throughout the system components. All of the above measuring processes were monitored by a computer-based data-acquisition system. The collected data was recorded at every one second interval in a data logger, which was later used for analysis **Fig.3 [16]**.

4. Experimental methods and procedure

In general, the multi-mode-functional DX-SAHP system can offer two fundamental operating modes; Space heating only mode and it can also produce domestic hot water and space heating mode. The switching between those two modes is by means of valve position and on–off controls. There is a two-way solenoid valve **Fig.3 [13]**, one way non reversing valve on the refrigerant pipes at the locations shown in **Fig.3 [14].** A control box was employed to determine and govern the operations running and modes of the system, which was supplied with digital cabinet outputs to organise the compressor's frequency **Fig.3[12]**, on–offs of valves, and other to control the pressure relationship between the temperature of the plates and solar simulator cut-off. Two pressure gages were also used to measure the hot cycle side and cold side 'charging and discharging line' **Fig.3[15]**.

For about two months from February to late March 2016, experiments were carried out for the two fundamental operating modes to investigate the performance of the multimode-functional DX-SAHP system during the winter season. The following parameters have been measured: the whole system including electric power consumed by the compressor, pump, solar irradiations on the collector/evaporator; fans and other electric power consuming elements; temperatures of both the R407c as working fluid loop and water loop at different locations, inlet/outlet absorber plate, the

water in hot domestic tank, air at heat pump inlet and air at heat pump outlet; flow rate of the water loop; pressures of refrigerant outlets of compressor, evaporator and condenser. All parameters were recorded at each 1 second using data logger.

5.1 Space-heating-only mode

This mode can be used to provide the room with space heating during the cold season, when heating of the room air is essential. At this mode, the refrigerant-filled solar collector array on the expected roof acts as an evaporator, while the finned coil tube heat exchanger works as a condenser. The refrigerant vapour from the compressor enters the heat exchanger directly. The centrifugal fan was used to dissipate the heat to the room, and meanwhile the water-to refrigerant heat exchanger is switched off. As a part of the control strategy, the heat pump operates only from 20:00pm to 04:00am, because of targeting low outdoor temperatures to reach certain conditions; the collector's temperature is below the ambient temperature. On the other hand the water circulation pump was stopped and the water loop closed.

Using the space-heating-only mode, the function of producing hot water is inefficient, and the system COP for space heating at any time (t) is defined as (Kuang and Wang 2006);

$$COP_{h\text{-}sys}\,(t) = \frac{Q_h(t)}{W\,(t)} \qquad (1)$$

Where: Q_h (t) is the heat exchange rate in the plate condenser, and W (t) is the system power input. If W (t) is defined as the power input for compressor, the rate from equation (1) is so-called the heat pump COP. Within the duration of operating period τ, while the average COP_h-sys is defined as

$$COP_{h\text{-}sys,av} = \frac{\int_0^\tau Q_h\,(t)\,dt}{\int_0^\tau W\,(t)\,dt} \qquad (2)$$

5.2 Space and water-heating mode

This mode is used for both hot water and space heating production. At this mode, the two-way valve is positioned after the compressor serves as two fluid lines to feed both heat exchangers through bypassing the refrigerant flow. The water in the hot domestic tank (DHWT) is heated up to 60 °C through water-to-refrigerant plate heat exchanger. The immersed condenser coil-tube dissipates heat to the water tank. Meanwhile the water pump on the loop is powered-on. Whereas rejected energy by the finned-coil tube condenser contributes to space heating. In this operation the solenoid valve shuts the water loop side down once the water temperature in the tank exceeds the load temperature (60 °C). This makes the refrigeration cycle operate in a steady state condition except the storage tank.

The COP for space and water-heating mode is defined as(Kuang and Wang 2006);

$$COP_{w\text{-}sys}\,(t) = \frac{Q_w\,(t)}{W\,(t)} \qquad (3)$$

And

$$COP_{w\text{-}sys,\ av}=\frac{\int_0^{\tau} Q_w\,(t)dt}{\int_0^{\tau} W\,(t)dt} \quad (4)$$

Where: Q_w (t) is the heat exchanger rate at the water storage tank.

6. First law thermal analysis

When the solar radiation with intensity of (see Appendix A) falls on the solar collector, a main part of the radiation (I), strikes to the aluminium absorber plate electroplated with black paint selective coating. A part of solar radiation is absorbed by the working fluid ($Q_{evaporator}$) and the remained part is dissipated through top and bottom of the absorber plate to the surrounding. In other words, to compute the outlet temperature and efficiency of the solar collector, first the heat losses to surrounding should be calculated. The rate of useful energy extracted by the collector experimentally (Qevp) expressed as the rate of extraction under steady state condition is proportional to the rate of useful energy absorbed by the collector was more than the energy lost by the collector to its surrounding. The relation between the absorbed heat and heat losses are as follows:

$$Q_{evaporate}=Ac * \left[\tau \propto I - U_L(T_p - T_a)\right] \quad (5)$$

$$= F'\ Ac\left[\tau \propto I - U_L(\check{T} - T_a\right] \quad (6)$$

Where:

Ac: Solar collector's surface area (m²)

∝: The collector's absorption rate 0.9

I: The intensity of the solar radiation in (W/m²)

U_L: The collector's overall loss coefficients (W/m²)

T_p: The collector/evaporator temperature (°c)

T_a: Ambient temperature (c°)

F': Solar collector's efficiency factor which is depended on tube-and-sheet

$\check{T}$: Mean refrigerant temperature in the collector/evaporator (°c)

By assuming that the losses of the plates/collectors occur to a common sink temperatureT_a, parameter U_L that is the overall heat loss coefficient can be determined as:

$$U_L = U_t + U_b + U_e \quad (7)$$

Where U_t the heat loss coefficient from the top/plate, U_b is the heat loss coefficient from the bottom/plate, and U_e is the heat loss coefficient from the edges of the collector. To calculateU_t, the following correlation can be used:

$$U_{top} = \left(\frac{N}{\frac{C}{Tp}\left[\frac{Tp-Ta}{(N+f)}\right]^{e}} \right)^{-1} + \frac{1}{h_w} + \frac{\sigma(Tp+Ta)(Tp^2+Ta^2)}{\frac{1}{\varepsilon_{p+0.0091Nh_w}} + \frac{2N+f-1+0.113\varepsilon_p}{\varepsilon_p} - N} \quad (8)$$

Where N is the number of glass covers that for present paper is 0, σ is Stefan-Boltzmann constant, and ε_p is emittance plate, the parameter of h_w is the wind heat transfer coefficient and V_w is wind velocity and L is the length of collector can be calculated by:

$$h_w = \frac{8.6V_w^{0.6}}{L^{0.4}} \quad (9)$$

$$C = 520 * (1 - 0.0000\beta^2) \text{ for } 0° < \beta < 70°; \text{for } 70° < \beta < 90°, \text{use } \beta = 70° \quad (10)$$

$$f = (1 + 0.89h_w - 0.1166h_w\varepsilon_p)(1 + 0.07866N) \text{ In which } \beta \text{ is the collector slope.} \quad (11)$$

Note that the main heat losses occur from the top. To determine the heat losses from the edges is out of scope for this paper, as for the bottom layer, the following equations can be used:

$$U_{bottom} = \frac{1}{\frac{t_b}{k_b} + \frac{1}{h_{b.a}}} \quad (12)$$

Where k_b and t_b are the thermal conductivity and thickness of insulators bottom edges respectively and $h_{b.a}$ is convection heat transfer coefficient bottom and edges, and their values are assumed to be the same and equal to =h_w=5 W/m²°c for still air. As seen, to calculateU_t, and, thusU_L, the value of T_p should be determined at first. For this purpose, an initial value of T_p is measured experimentally, and the quantities of U_L and Q_{Solar} are calculated. Q_{Solar} can be computed through modelling via refrigerant enthalpy chart:

Where $Q_{evaporator}$ via experiment laboratory experiment $\simeq$ Q_{Solar} via modelling

$$Q_{Solar} = \dot{m}_r * (h_{refout} - h_{refin}) \quad (13)$$

$$Q_{Solar,ref} = \dot{m}_r * (h_2 - h_1) \quad (14)$$

Where:

$\dot{m}_r$: Collector mass flow rate $(k_g * s^{-1})$, $\dot{m}_r = Q * \rho$ wherein $Q = \frac{\pi}{4}D^2 * V$ (15)

Q: The volumetric flow rate $(m^3 * s^{-1})$ (16)

D: Outer tube diameter of risers (m)

ρ: Fluid density $(k_g * m^{-3})$

V = The mean velocity of the fluid $(m * s^{-1})$

h_{refout}: Refrigerant/Collector outlet enthalpy $(k_J * k_g^{-1})$

h_{refin}: Refrigerant/ Collector inlet enthalpy $(k_J * k_g^{-1})$

For this work, it is not necessary to develop a completely new analysis for the tube-sheet relation situation, Hottel-Whilliar-Blis have developed the collector efficiency factor F'(Duffi & Beckman, 2006[*]), for the tube-sheet relation in the formula as following:

$$F'=\frac{1}{W\left[\frac{1}{[D+(W-D).F]}+\frac{W.U_L}{\pi D_i hf_i}\right]} \quad (17)$$

Where:

W: Pitch between the serpentine tubes of the collector

D: Outer tube diameter of risers

D_i: Inner tube diameter of risers

F : Fin efficiency factor of the collector plate = $\frac{\tanh[m(W-D)/2]}{m(W-D)/2}$ (18)

$$m=\sqrt{U_L/k_m * \delta_m} \quad (19)$$

Where:

k_m: Thermal conductivity of the collector/evaporator flat plate (211 W/m°c)

δ_m: Thickness of the absorber collector/evaporator flat plate (0.002 mm)

To obtain the internal heat transfer coefficient (h_{fi}), the definition of the Nusselt number must be applied:

$$hf_i = \frac{N_u * k_{ref}}{D_i} \quad (20)$$

Where:

N_u: Nusselt number a dimensionless parameter used in calculations of heat transfer between a moving fluid and a solid body

k_{ref}: Refrigerant thermal conductivity (W/m°c)

To calculate the Nusselt number, Gnielinski correlation is used that is valid for $3000 \leq Re \leq 5 \times 10^5$ and $0.5 \ Pr \leq 2000$, this correlation is expressed as:

$$N_u=\frac{(f/8)(R_e-1000)*P_r}{1+12.7(f/8)^{0.5}*(P_r^{0.6}-1)} \quad (21)$$

Where f is Darcy friction factor and can be obtained by Petukhov's formula for evaluating it, assuming that any quality change in the collector/evaporator is largely due to enthalpy change and neglecting the quality difference due to pressure drop. This result is relatively acceptable for turbulent flow in smooth pipes:

$$f' = \frac{1}{[0.790 I_n(R_e)-1.64]^2} \quad (22)$$

The relation is valid for the Reynolds numbers between 4000 and 10^8, Reynolds and Prandtl numbers are described as:

$$R_e = \frac{4\dot{m}_r}{\pi . D_i . \mu_{ref}} \qquad (23)$$

$$P_r = \frac{\mu_{ref} . C_{p_{ref}}}{k_{ref}}$$

It should be noted that the Reynolds numbers is in terms of mass flow rate in any riser ($\dot{m}_r$) where (μ_{ref}) refrigerant viscosity ($k_g * m * s^{-1}$).

6.1 The evaporator/collector section

The collector model is used to determine the value of the outlet collector's temperature T_2 for given values of ambient temperature T_a andI_{coll} , refrigerant properties h_1 and h_4 and the heat pump parameters (specific volume v_1 and the displacement volume rate(VD)). The net energy absorbed by the fluid circulating via the collector/evaporator equals to the incident solar radiation minus the heat loss from the collector/evaporator, and accordingly the outlet fluid temperature T_2 can be calculated through the steady state energy balance on the collector/evaporator in modelling part, expressed by thereby:

$$\frac{VD}{v_1}(h_2 - h_4) = F'Ac * [I_{coll}(\tau \propto) - U_L(T_2 - T_a)] \quad (24)$$

From the above equation one can solve for T_2 as:

$$T_2 = T_a + \frac{I_{coll.(\tau\alpha)}}{U_L} - \left(\frac{VD}{v_1}\right) * \frac{(h_2 - h_1)}{U_L . F' . A_c} \qquad (25) \text{ (For modelling part)}$$

For a given location (Nottingham, UK), all the data explained (Table: 2) are provided as inputs. The value of the collector/evaporator temperature at given time of the day is measured experimentally and compared to those assumed values of enthalpies at state points 2 and 1 which are modelled and computed from the polynomial fit for the refrigerant properties. New values of T_2 according to circulated processes are compared with the previously measured experimental results and modelled values of T_2. The values of these parameters are incorporated over a given month. The thermal energy produced by the heat pump Q_H (W) is calculated from the following equation:

Table 1: Standard system parameters for thermal analysis

Parameter	Value
1 Condensing temperature	86 °c(variable)
2 Collector area	4.22 m²
3 Collector efficiency factor	0.947 (variable)
4 Transmittance-absorptance product	0.9
5 Collector heat loss coefficient= 9.999 W/°c m²	
6 Compressor efficiency	0.75 (variable)
7 Compressor displacement=7.84E-04 m³/s	

$$Q_{H\_ref} = \dot{m}_{coll\_ref}(h_3 - h_4) \qquad (26)$$

$$Q_{H\_air} = \dot{m}_{air} * C_{p\_air}(T_{out} - T_{in}) \quad (27)$$

Where $\dot{m}_{coll\_ref}$ and $\dot{m}_{air}$ are the collector's refrigerant and condenser's rejected air mass flow rate respectively, whereas C_{p_air} is the air specific heat capacity. Consequently, the efficiency of the solar-collector η_{coll_ref} can be defined both experimentally and in model part as expressed below:

$$\dot{m}_{coll\_ref} = \frac{V_D}{v_1} \ (kg * \ S^{-1}) \qquad (28)$$

$$\dot{m}_{air} = \rho * V * A \ (kg * S^{-1}) \qquad (29)$$

Where ρ is density of flowing air $(k_g * m^{-3})$, V is the air flow velocity $(m/_s)$ and A the flow area (m^2)

$$\eta_{coll\_ref} = \frac{Q_{solar}}{I_{coll} * A_c} \qquad \text{For modelling part (30)}$$

$$\eta_{coll\_ref} = \frac{Q_{evaporator}}{I_{coll} * A_c} \text{ For experiment part (31)}$$

6.2 The compressor section

The compressor work W_{comp} or compressor power $W_{power} = \dot{m}_{refrigerant} * W_{comp}$ for a given pressure ratio P_2/P_1 is determined for the modelling part from expression:

$W_{comp} = \frac{P_1 v_1}{\eta_{comp}} \left(\frac{k}{k-1}\right) \left[\frac{P_2}{P_1}\right]^{\frac{k-1}{k}} - 1]$ Or $W_{comp} = \dot{m}_r(h_3 - h_2)$ For model part (32)

$W_{comp} = \frac{Work_{electronic}}{\eta_{comp}}$ for the experimental part, the compressor and auxiliary power devices electricity-consumption displayed on the power-meter was recorded. (33)

Where [k] is the ratio of specific heat, and for R-407c it has a value of Eq.8. The assumption of ideal gas behaviour during the compression process appeared to be reasonably acceptable since the compressor's work computed under such assumption is slightly overestimated in comparison with the compressor's work calculated instantly through the experiment work. While $P_{2/}P_1$ can be determined through the measured high side and low side pressure respectively from the test rig; as for the modelling section, via refrigerant thermodynamic polynomial chart. The work of the compressor also relied on the efficiency of the compressor which is a variable related to fluid condition (entropy), and temperature of the collector outlet fluid T_2 (enthalpy).

$\eta_{comp} = \frac{T_{2i} - T_2}{T_{2a} - T_2}$ (Efficiency of compressor), therefore the iteration of calculated η_{comp} and their repetitions in turn depends yet again on fluid state arising out of T_2 variation, as well as to define the exact compressor's efficiency(η_{comp}). The situation here changes very rapidly when T_{2i} isentropic (CTD calculated) and T_{2a} each of which changes its temperature:

$$T_{2i} = T_2 * \left[\frac{P_2}{P_1}\right]^{0.28571} \qquad (34)$$

$$T_{2a} = T_{3'} = T_2 \left[\frac{P_2}{P_1}\right]^{\left[\frac{n-1}{n}\right]} \quad (35)$$

Where $n = k$, while $T_{3'}$ "discharge compressor temperature(°C)" and $\eta comp$ is neglected. To determine the liquid temperatures' after compressor T_3 operation can be calculated are as follows

where the compressor's $\eta comp$ was provided previously according to variable solar radiation incidents.

$$T_3 = T_2\left[1 + \frac{\left[\frac{P_2}{P_1}\right]^{\frac{[k-1]}{k}} - 1}{\eta comp}\right] \quad (36)$$

Calculating modelling section T_3 is determined to count energy provided by compressor as aforementioned, since the coefficient of performance of the heat pump (COP_H) is inversely dependent on compressor's work is calculated from equation listed below.

$$COP_{heatpump} = \frac{Q_H}{Work_{comp}} \quad (37)$$

Q_H The thermal energy produced by the heat pump which is the condenser work $(Q_{condenser})$ and will be discussed in the next section.

6.3 The condenser section

The air velocities were measured so as to further obtain the air flow rate at the outlet of condensation fan and the heating capacity. The operating performance of a heat pump is related to the temperature that is the difference between the temperature of the heat source and the output temperature of the heat pump. Therefore, the $COP_{heat\ pump}$ determined solely by the condensation temperature and the temperature lift (condensation-evaporation temperature). The real heating capacity is obtained from equation [38] by measuring the air temperature difference between inlet and outlet of and the air mass flow rate at outlet orifice.

$$Q_{condenser_{air}} = \dot{m}_{r_{air}} * c_{p_{air}}(T_{out.condeser} - T_{in.condenser}) \quad (38)$$

Since the system requires auxiliary energy owing to intermittency during night-time or absence of available solar energy, the effective coefficient of performance and seasonal performance factors are determined as:

$$COP_{effective} = \frac{Q_{condenser\ (air)}}{Work_{electronic}} \quad (39)$$

From the above equation one can solve for

$$\text{Effectiveness} = \frac{Q_{heatpump}}{Q_{heatpump} * Q_{electronic}} = \frac{Q_H}{W} \quad (40)$$

$$\text{SPF} = \frac{\text{Heat energy output (kWh)}}{\text{Total input energy (kWh)}} \quad (41)$$

6.4 Thermostatic expansion valve

An orifice thermodynamic expansion valve is modelled, through which the refrigerant is extended from condensing to evaporating pressures. Liquid mass flow rate passing thought it can be formulated as follow:

$$\dot{m}_r = C_v A_0 \sqrt{2_{\rho i,I} \Delta P} \quad (42)$$

Where C_v is liquid flow coefficient, which depends on the valve opening degree, and when the valve is fully open, it can reaches its maximum value; C_v is evaluated by (Wile 1935) empirically = $0.02005\sqrt{\rho i, I} + 0.634 v_0$ (43). While A_0 is the minimum flow area across the orifice. Whereas, v_0 is the refrigerant specific volume at the outlet valve. $\rho i, I$ is the density of the liquid that can be calculated at the valve inlet. ΔP is the variation of the pressure across the orifice valve.

For the process of an isenthalpic in expansion device, the following equation is achieved:

$$h_3 = h_4 \tag{43}$$

Where; h_3, h_4 are the refrigerant's specific enthalpies at valve inlet and outlet.

6.5 Condenser/Domestic hot water storage tank (DHWT)

Serpentine copper tube is used for hot water tank condenser, which is immersed in the (DHWT). Similarly to collector/evaporator, the condenser copper tube can also be divided into sections equal with enthalpy difference. Supposing that the DHWT is non-stratified, energy balance can be obtained with the immersed condenser as follow:

$$Q_w = M_w C_{pw} \frac{dt_w}{d_\tau} = \mathfrak{m}_r (h_2 - h_3) - U_{L,t} A_t (t_w - t_a) \tag{44}$$

Where Q_w is the condenser's gained heat, which is released and transferred heat rate to the DHWT by the condenser. M_w is the water mass in the water tank, C_{pw} is defined as the water specific heat, while t_w is the water temperature, whereas τ is the time, and h_2, h_3 is the refrigerant's specific enthalpies at the condenser's inlet and outlet respectively. The total water tank heat loss coefficient is $U_{L,t}$ and A_t is the total heat transfer area of the wall of the water tank.

7. Experimental results and analysis

7.1 Thermodynamic cycle

To achieve constant quasi-steady heat pump condition by means of constant temperature and condensation, the work is sufficiently enough to meet the minimum requirement for and to the heat pump, therefore, allowing it to operate reversibly and to determine the COP of the heat pumpFig.5. In the current study analytical investigation were considered in order to examine the thermodynamic performance of the cycle along with experimental running tests to validate the modelling part. The enthalpies of the refrigerant R407c as functions of pressure and temperature can be found in the Table.2

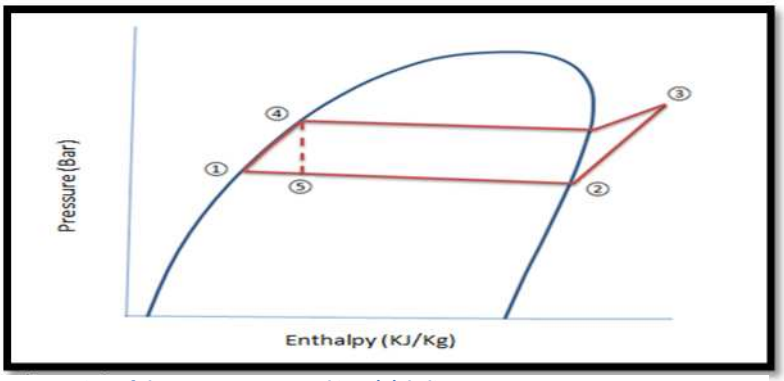

Figure 5: The vapor compression of the system presented in a (*p*)-*h* diagram

The current study carried out a system analysis for multi-mode-functions DX-SAHP to match component rules and understanding its performance and analysis. Variant COP with correlation with different irradiation intensities and several water flow rates have been taken into account and their characteristics have been studied. Experimental data are then compared with the analytical results. The impact of various system parameters on the response on the water temperature variation in the heat storage tank, indoor air temperature of the building, electrical power consumption and heating capacities of the system were investigated. Experimental data including operation control, system matching and component design were relatively obtained, which are more likely to play a considerable role for such systems to further studies and applications. The present system is designed and fabricated locally at laboratory in the University of Nottingham UK. The schematic diagram is shown in Fig.1

7.1 Space-heating-only mode

Multimode-functional DX-SAHP system was tested on the lowest three consecutive days during February and March 2016 respectively, at space-heating mode with the average of daily-outdoor air temperatures (Ta,av) ranging from 6.5 to 8.2 °C and solar simulator were exposed on the collector has varied from 0, 57, 100 and 200 W/m². The experimental data are listed in Table. 1. In order to examine the DX-SAHP system capability of space-heating, the temperatures of indoor rejected air was recorded during the testing period; in the present study, thermal camera has been chosen to analyse the temperature differences between the surfacesFig.6.

Table.1

Performance of DX-SAHP space-heating mode									
	W/m²	T_{room} (°C)	$f$comp (Hz)	HR,av (°C)	Inlet air,av (°C)	Qcond_air,av (W)	Low_pressure-bar	High_pressure-bar	COP-sys,av
	0 W/m²	18.35	45-50	24.9	7.48	3021.168	1.1	9.8	2.842115
	0 W/m²	19.14	45-50	26.6	8.23	3185.927	1.3	10	2.99711
	0 W/m²	19	45-50	25	8.5	2861.612	1.1	10.3	2.692015
	57 W/m²	18.8	45-50	25.3	6.55	3191.13	1.3	11.4	3.860737
	100 W/m²	20.1	45-50	25.25	6.9	3182.459	1.4	11.5	3.877208
	200 W/m²	19.8	45-50	25.6	7.5	3139.101	1.5	11.6	3.939562

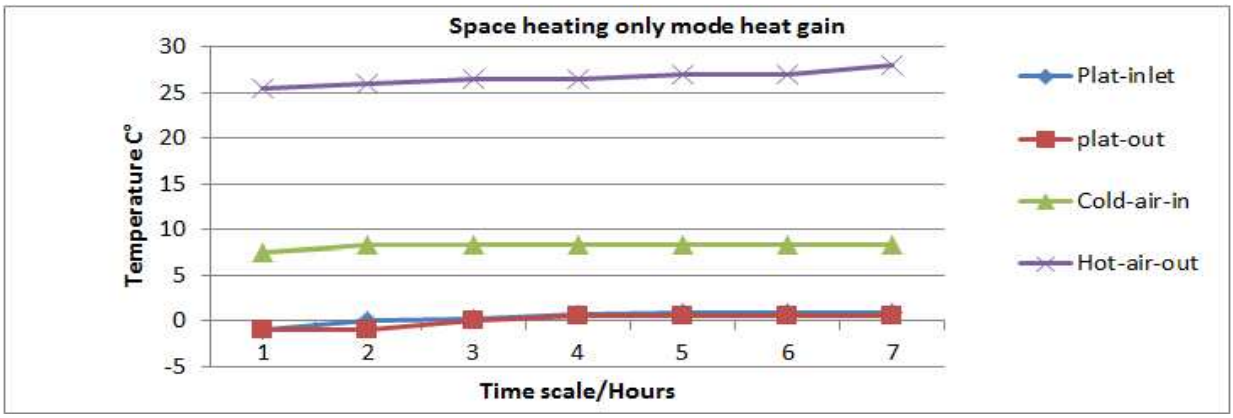

Figure 4-1 Comparison between room temperature (HR) and inlet/outlet, cold air temperature

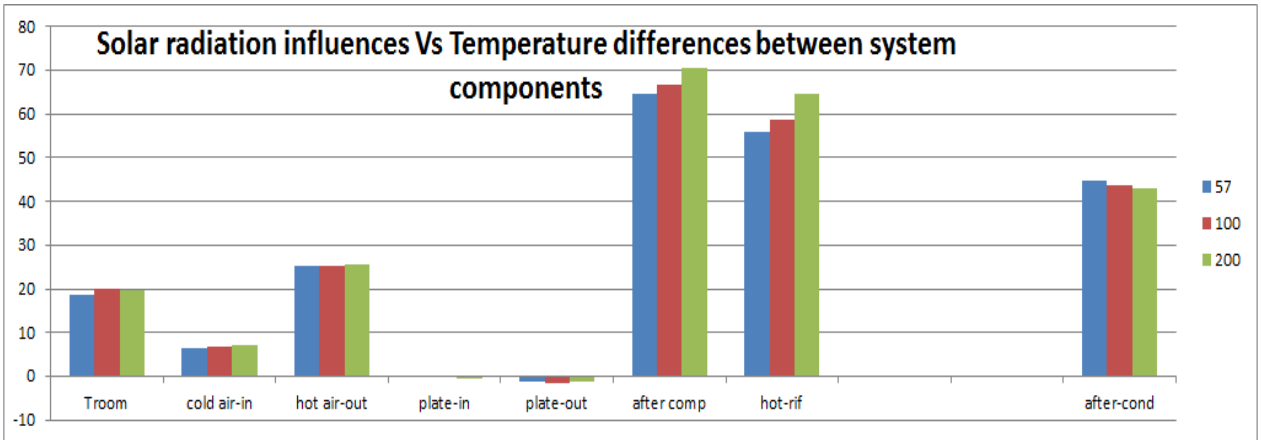

Figure 4-2 variations of temperatures between room, inlet/outlet and compressor liquid in/out under different solar intensity

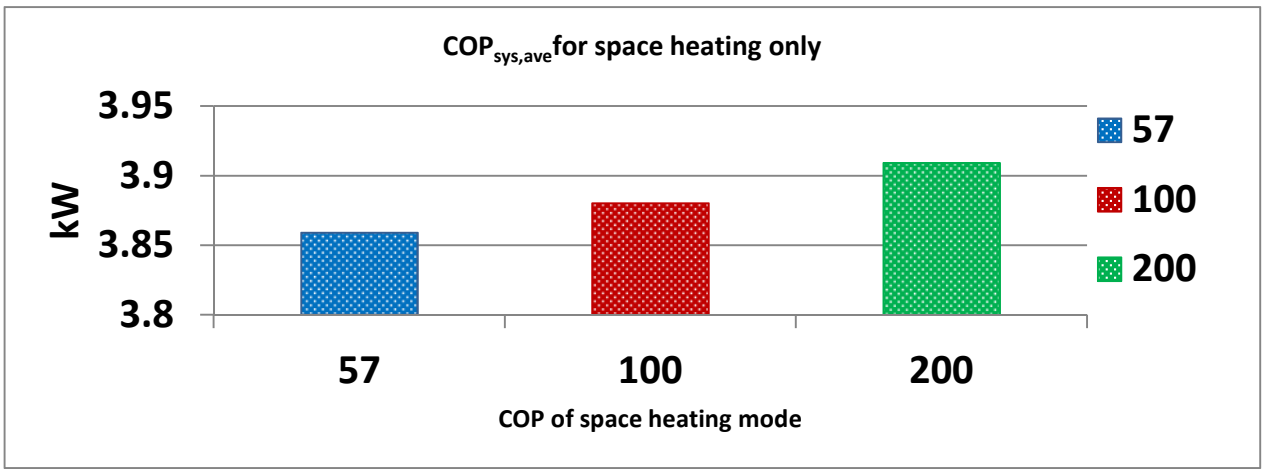

Figure 4-3 COP average of the system at different solar intensities in space heating mode only

During the experiment, Matlab model analysis was used to perform a mathematical process using model data to validate the experimental workFig.5. This is shown in the results that the Qcond_air, av in the experimental work is slightly different from the theoretical values; however the differences are only up to 4% maxFig.[4-3]. Fig. 4-1 shows the monitored data consecutively recorded using data logger for the produced heating air by the system as heating room (HRave) or hot-air-out in the space-heating mode during the lowest outdoor temperatures at specific dates in winter. The results indicated that the average of Qcond_air, av, av is up to 3 kW in the whole experimental results, while produced hot air is between 25-26 °C. Indoor air temperature at both the 0 W/m² and different irradiation intensities remained the same, with given identical experiment parameters. Experiments are taken under the condition that the solar irradiations are 57,100 and 200 W/m² and the temperature of the indoor temperature is 20°C/18°C (DB). The result shows that the enhancement of solar irradiation can effectively increase the evaporator temperatureFig.[4-3]. The energy consumption is swinging between 910W, 1000W and 1010W, respectively.

As the environment is stable, after nearly twenty-minutes, the system can reach quasi-operational-state. Under the outdoor temperature of 6 °C, 7°C and 8°C, the evaporation temperature is -1°C, 0°C and 1°C, respectively Fig. 4-1. The evaporator temperature decrease as the ambient (outdoor)

temperature decreases Fig. 4-2. Meanwhile, the evaporator temperature is always lower than the ambient, which leads to heat transfer from the ambient to the collector. It is also observed that the difference between the evaporator temperature and the ambient temperature is up to 7.0°C corresponding to the ambient temperature 6, 7 and 8°C. The COP of the DX-SAHP in the space heating only mode increases with the increase of the irradiation intensity, as Fig. 4-3 depicts, the specific values of the coefficient performance are 2.7kW, 3.86kW, 3.87kW and 3.9kW respectively, corresponding to 0 W/m², 57 W/m², 100 W/m² and 200 W/m². In addition, COP of the system increases as the solar irradiation increases. It is noticed that when the evaporator's temperature increases, the evaporating pressure, Table.1 as well as the refrigeration mass rate increases, causing the surge of the energy consumption of the compressor. It also shows the condensing heat exchanging rate under the four experiment conditions. The values are 3022.9W, 3191.1W, 3182.4W and 3139.1W. Fig.4-3. Under the tested conditions, COP is 2.84kW, 3.86kW, 3.877kW and 3.94kW. The increase of COP with the increase of the ambient temperature is not significant. However, as the condensing heat exchange rate increases; the energy consumption also increases and to some extent obstructs the increase of COP.

7.2 Space and water heating mode

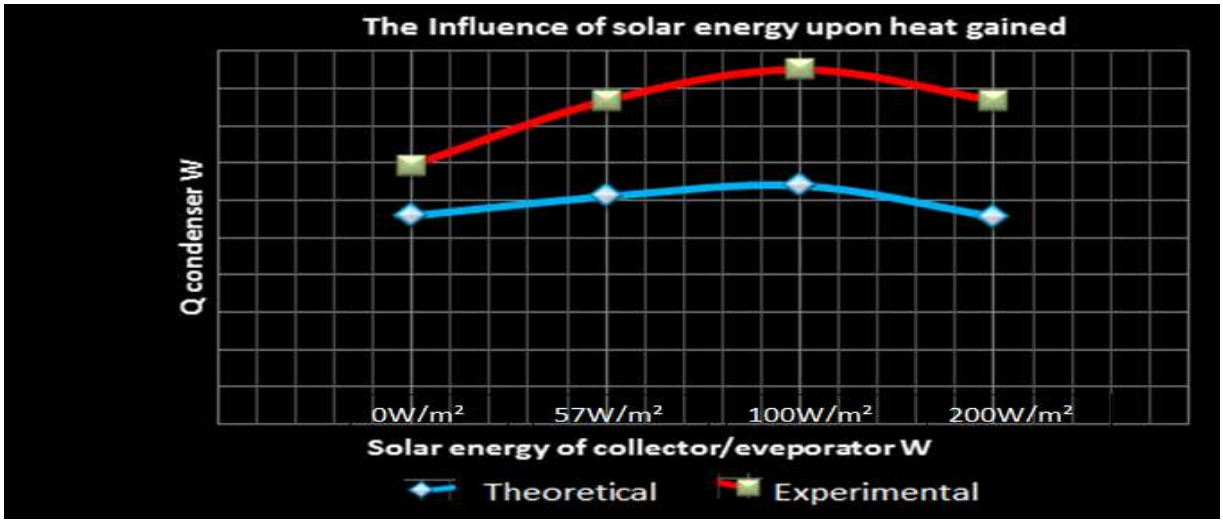

Figure 4-4 Comparison between Theoretical and Experimental of the DXSAHP system performance under different irradiation

water flow	W/m²	T_{room} (°C)	$f$comp (Hz)	HR,av (°C)	Inlet air,av (°C)	Qcond_w,av (kW)	Low_pressure-bar	High_pressure-bar	COP-sys,av
1LPM	0 W/m²	18.35	45-50	24.9	7.48	1143.069	3.4	21	2.842115
2LPM	0 W/m²	19.14	45-50	26.6	8.23	836.3916	3.4	21	2.99711
3LPM	0 W/m²	19	4-550	25	8.5	487.8951	3.4	21	2.692015
2PLM	57 W/m²	18.8	45-50	25.3	6.55	320.6168	3.5	22	3.860737
2PLM	100 W/m²	20.1	45-50	25.25	6.9	348.4965	3.5	22	3.880208

2PLM	200 W/m²	19.8	45-50	25.6	7.5	418.1958	3.5	22	3.911562

The experimental data listed in Table. 2 are taken from the space/water heating mode. In this case, the total volume of hot water is about 200 litres, with the nominal temperature is chosen to be 50 °C. The system's performance is governed significantly by the change of solar irradiation and ambient air temperature. For instance, the COPsys, av for this mode is much enhanced with the increase in solar irradiation and ambient temperature. The refrigerant flows through two-way solenoid valve, one of the directions feeds into the finned tube condenser, leading to reject heat, thus producing space heating. Meanwhile, the second direction is to supply hot refrigerant to the plate heat exchanger to heat up the water inside the DHWT for water heating purposes. The solenoid valve controls the water cycle by sending signals through embedded heat sensor into the water tank to maintain the required temperature.

Table.2 shows the typical ambient (Troom) and inlet air, av (outdoor) temperature during the operational period between (8:00pm-4:00am). Different solar radiation and water flow rates are implemented to investigate the system, the compatibility between different components is critical for maintaining high performance. In the DX-SAHP system, the thermal storage tank is utilised to store hot water for domestic hot water during the winter. Water temperatures from the exchanger plate cycle (hot-water) to energy storage tank (DHWT) are plotted for specific time of the day in the experimental study under several radiations Figure.5. As shown in Figure.6 the outdoor temperature reached the maximum of 5.1 °C during experimental conditions, while various water flow rates were gauged and the refrigerant post compressor and at heat exchanger plate were measured Figure.7.

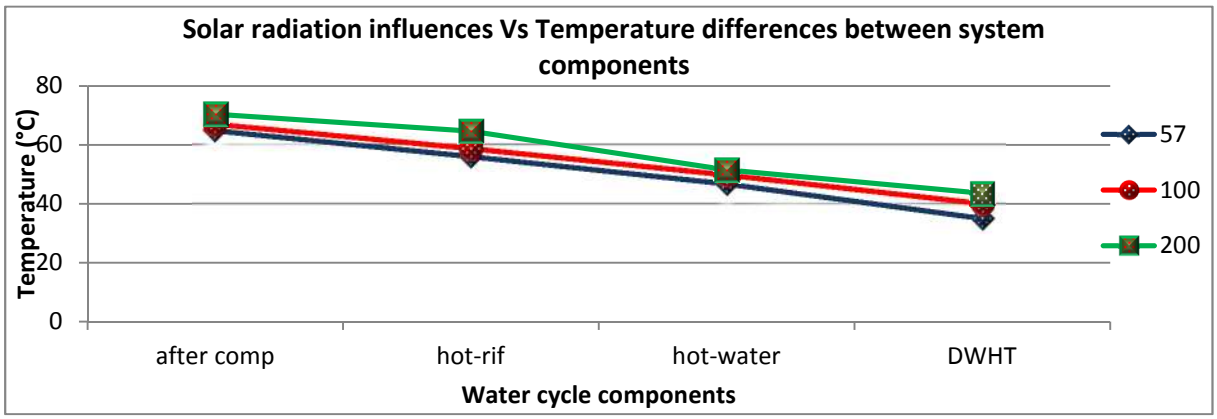

Figure 5 Solar irradiation influnces on the cycle performance

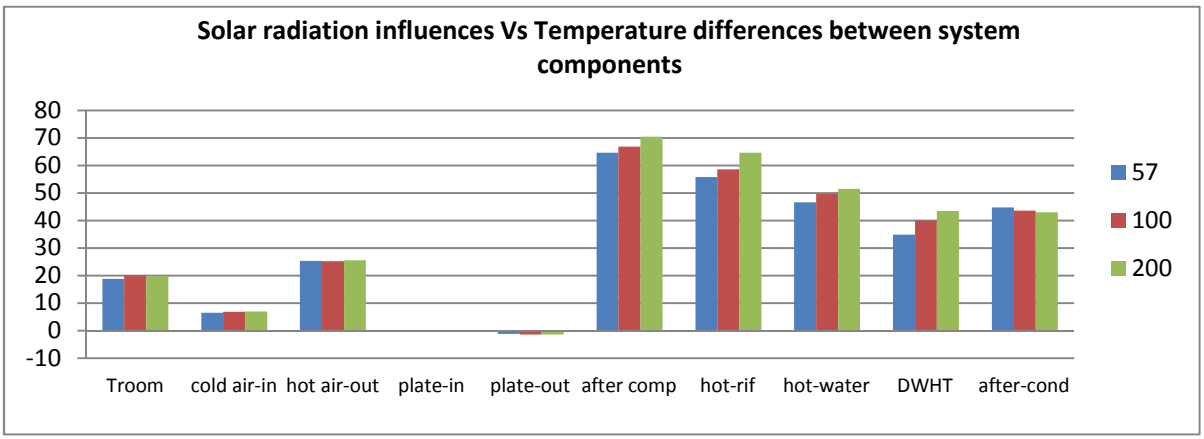

Figure 6: The effect of solar irradiation on the cycle equipment

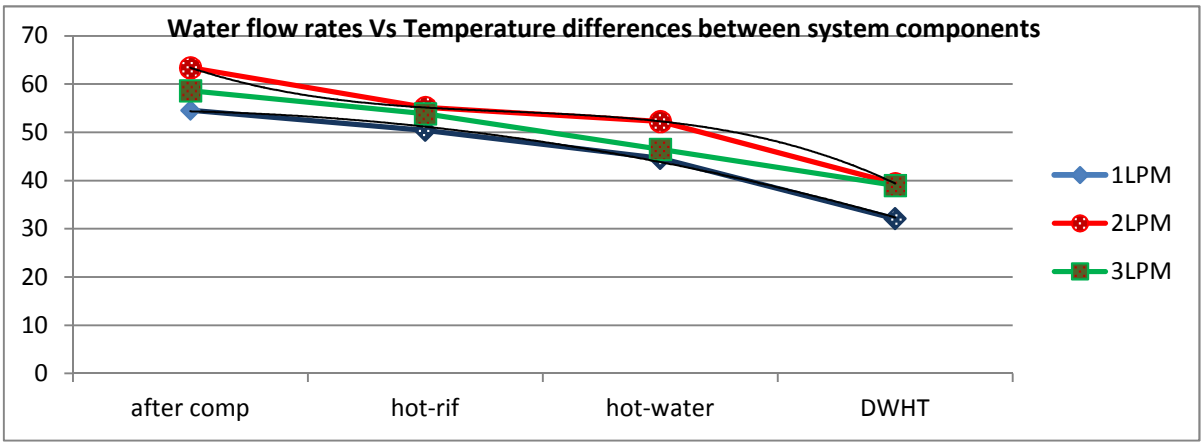

Figure 7: The effect of water flow rates of cycle equipment

It is obvious that at 200W/m², the hot water at the exchanger plate reaches its maximum temperature up to 53°C after two hour of running the system at exchanging fluid plate and after which the water starts passing through piping works, and water pump to DHWT. The quasi-static water temperature at the domestic hot water tank is 50°C Figure.6. Adjustable water flow rates were installed; Figure.7 showed that 1LPM is an optimal selection for the system space/water heating mode with 70 percent for space heating and 30% for water heating capacity Figure.8. The Qcond-air, are 3021.2W, 3186W, and 2862W respectively related to water flow rates, while Qexch-w about 1143.1W, 836.4W and 488W consecutively Table.3. COP's of the whole system slightly changed from 3.92, for 1LPM, to 3.80 for 2LPM and 3.20 for 3LPM.Whereas, the air and water COP's averaged between 2.84 for air and 1 respectively.

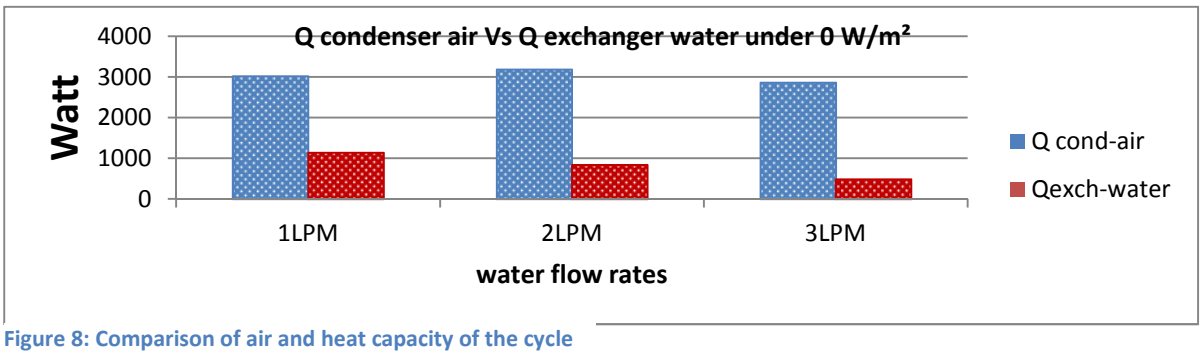

Figure 8: Comparison of air and heat capacity of the cycle

Table.3	*Q cond-air*	*Qexch-w*	Cop_{Sys}	*Totalenergy*	*%air*	*% water*	Cop_{air}	Cop_{water}
1LPM	3021.168	1143.069	3.917438	4164.237	72.55035	27.44965	2.842115	1.075323
2LPM	3185.927	836.3916	3.783931	4022.319	79.20623	20.79377	2.99711	0.786822
3LPM	2861.612	487.8951	3.150994	3349.507	85.43382	14.56618	2.692015	0.458979

Figure.9 clearly shows the monitoring temperature of the system's components under three water flow rates during the experimental period. The outdoor temperatures averaged between 5-8°C, whilst the refrigerant at the inlet of the evaporator (plates) between -3 to ±0 °C and at outlet swinging between -1.5 to 1°C. Figure.10 shows the relationship between the solar irradiation, temperature and COP on the space/water heating system mode.

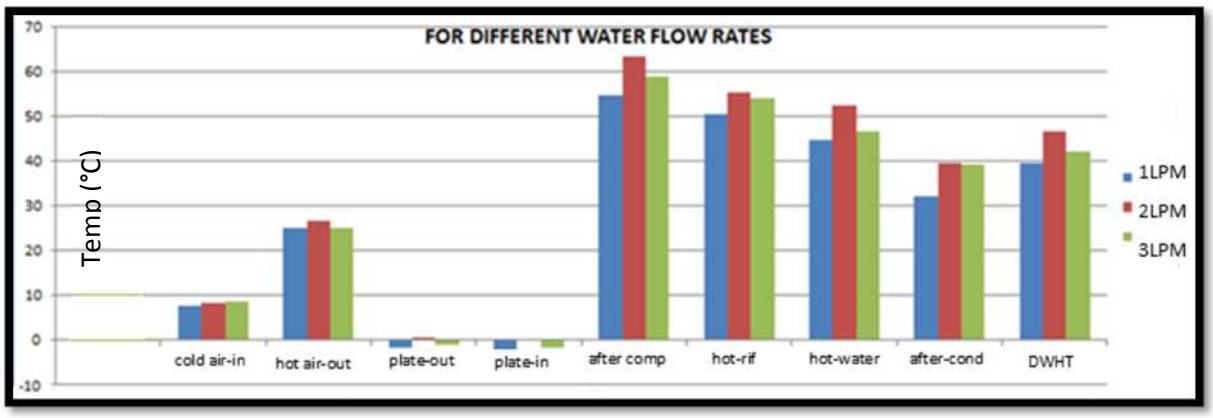

Figure 9: The effect of water flow rates of the whole system

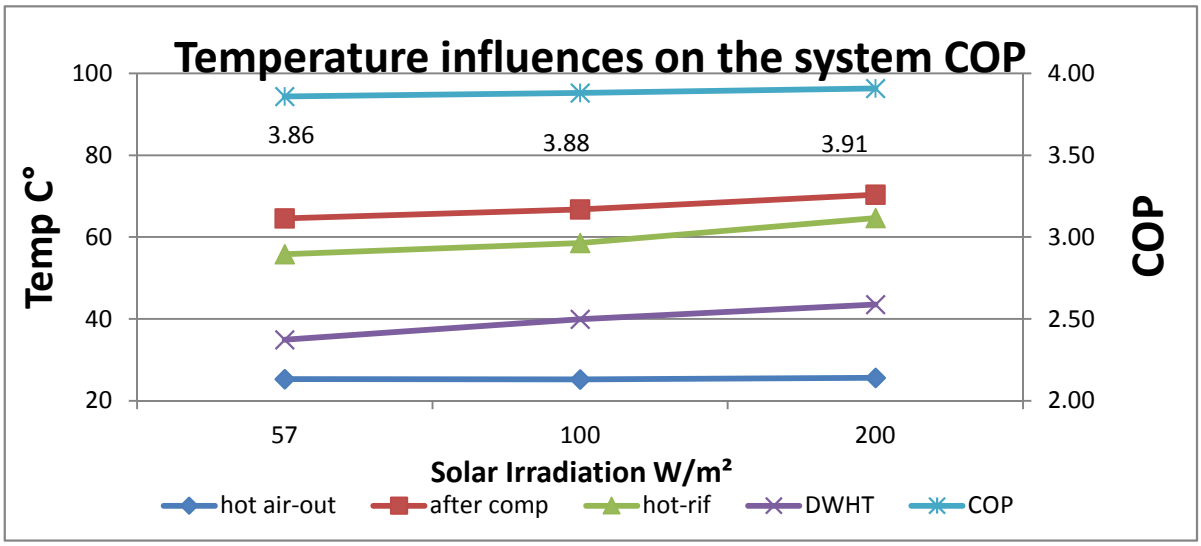

Figure 10 COP's of the system two cycles

8.The analysis of thermal camera on the system

In the current study, to investigate the influence of solar irradiation on the frosting effect and heat performance on the components surfaces thermal camera was used. In order to provide a comprehensive understanding of the operating conditions of the equipment through condition-based assessment and monitoring critical consideration. Equipment-operation data is gathered and analysed to show trends in performance and component characteristics. Data collected from monitoring equipment is analysed on regular basis to determine if values are within acceptable tolerances. The three flat plates, pump, pipe works, compressor, heat exchanger plates and expansion vessel, are pictured during the experiment. Excluding the solar irradiation, after 30 min, the surface of the absorb plates of the evaporator is covered by a layer of frost and the copper pipe of the outlet of the evaporator is frosted, as shown in Figure.11 (A-6, 7, 8), and as the experiment continues, the frosting will be more prominent. Whilst with solar irradiation of 100 and 200 W/m², the evaporator is partially frosted during the experiment Figure.11 (A-3, 4). Figure.11 (A-7, 2)

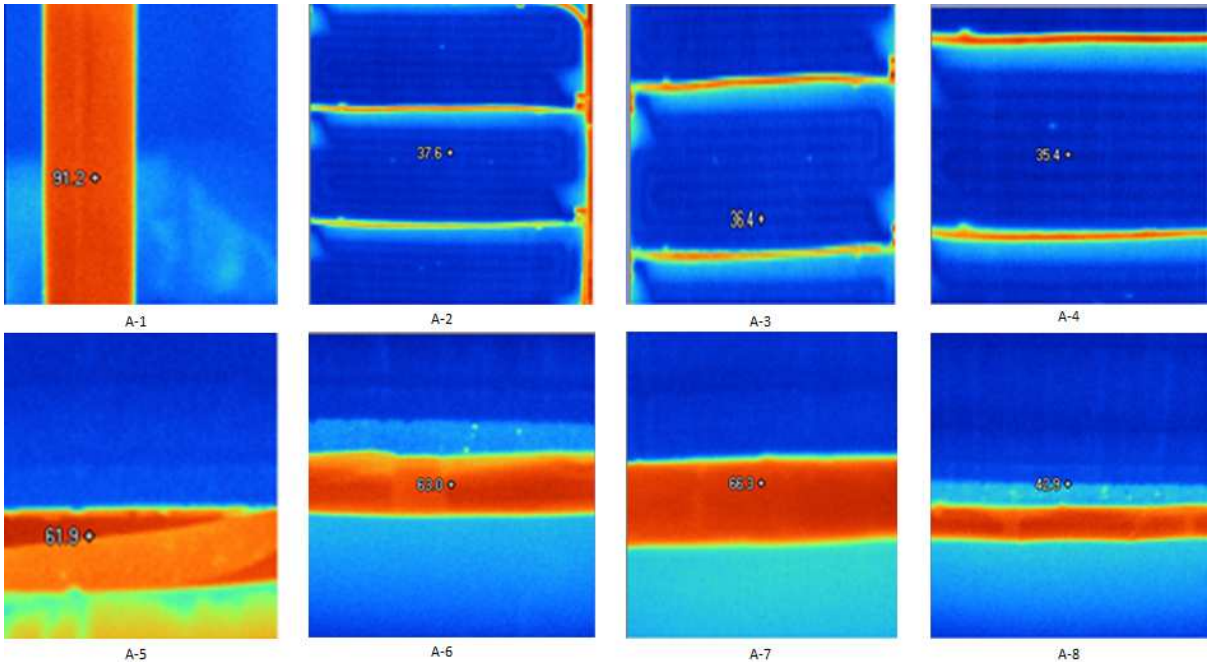

Figure 11: (A) Refractory performance of the system

By monitoring refractory performance over time, the hot spots on the thermal image depicts the mainstream of hot refrigerant pipe works, within which the fluid is absorbing the heat, thereby passing them from one plate to another all the way back to heat pump unit Figure.11. The compressor is significantly hotter than the other components Figure.11 (B-2, 3, 1), while the water to refrigerant heat exchanger plate, water pump and expansion vessel are respectively operating

warmer than the rest of the equipment. Figure.11 (B-4) clarifies the hot and cold water line in the water cycle. Natural convection is forced, with pump and fan occurs when warm refrigerant rises and cool refrigerant sinks. A blue (or dark) spot on the thermal image illustrates that the panels remain cold in order to absorb surrounding heat in a low temperature conditions. The lighter colored demonstrates frosty and cold area throughout the plates and system components Figure.11 (A-B).

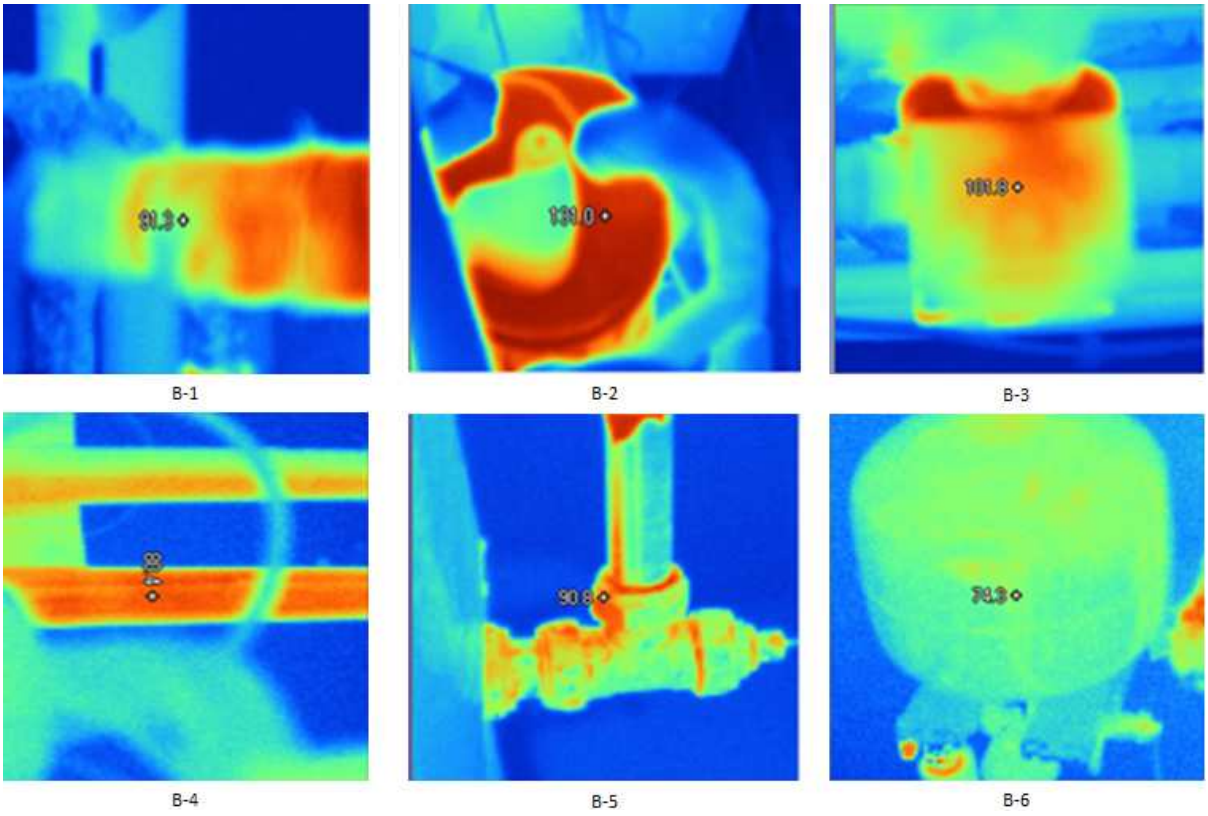

Figure 11: (B) Refractory performance of the system

9. Conclusion

DX-SAHP system was designed and fabricated at the university of Nottingham laboratory as aforementioned. It can offer multi-functions for residential uses, hot water supply and space heating in winter. To study the performance of Multi-functions DX-SAHP under different conditions, experiments were carried out in with solar simulator. The present study tests the system's real outdoor temperature of 4°C, 5°C, 6C°, 7°C and 8°C and solar irradiation is 0 W/m², 57W/m², 100W/m² and 200W/m² with different water flow rate; 1LPM, 2LPM and 3LPM. During winter time the experimental results show that the system operating in space heating only mode can produce adequate space heating during winter. According to the results, when the water temperatures in the condenser tank increase with time, the condensing temperature also increases. However, by modifying the system by adding water-to-refrigerant heat exchanger the performance is enhanced by cooling the liquid before it is passed through expansion valve, and corresponding COP and

collector efficiency values remain in steady state condition. Average values of COP ranged from 3 to 4 and solar collector efficiency was found to vary between 40% and 75% for water temperatures in the condenser tank varying between 43°C and 50 °C within two hours. Results indicate that the performance of the system is influenced significantly by collector area, and solar irradiation. Thermal images show that in any specific piece of equipment, when they are present there are no abnormal conditions as it goes through a complete operating cycle. In addition it is noticed that, the inner collector plate improves the collector's efficiency by absorbing the surrounding deplete heat at attic area and reducing its frost.. Energy input of the system increases because of solar irradiation, in addition, specific volume of refrigerant decreases and mass flow rate increases. This in turn leads to increase of the energy consumption by 5.6% and increase of the heating capacity of the system by 18.1% Off-peak electrical rates utilities can be used to reduce system energy consumption. The DX-SAHP system can supply 200L hot water with final temperature of about 50C daily under various conditions. Owing to the increase of heating capacity is more significant than that of energy consumption, COP is improved from 3.8 to 3.9 and the heating performance of the system improved accordingly. Therefore, solar irradiation can considerably reduce frosting formation of DX-SAHP and benefit the performance of the system. Multi-functional DX-SAHP system could guarantee a long-term operation under very low temperature and relatively low running cost.

For future studies, a larger volume compressor with higher speed can be replaced to keep abreast of enhancing the system performance, to achieve optimum steps in overarching refrigeration cycle.

1. Experimental Investigation on THS performance

2.1 Methodology

A testing rig, was designed and developed to investigate the sorption material performances to be used in the proposed sorption jacket. This system (see: Figures 1 a-b) was mainly designed to investigate the hydrodynamic and thermodynamic performance of the sorption material. Perforated tubes were used to facilitate vapour diffusion to the material thereby to reduce the effect of the reaction front and to provide uniform air flow. The reaction chamber (8) is rectangular shaped (500 mm x 250 mm x 200 mm) with a sloping roof to facilitate post absorbent airflow and is constructed of aluminium with welded seams.

Figure 1 (a) Schematic diagram and (b) view of the experimental test rig

Ten perforated tubes, d = 20mm, made up of 0.55 mm thick perforated aluminium sheet were placed vertically inside the reactor in two parallel rows with a horizontal distance, d = 100 mm between each (x and z direction) (See: Figure 2).

Figure 2 (a) Internal view of reactor showing perforated diffuser pipe allocation

The tubes are connected to an external manifold (12) to equalise airflow to each tube, with the top end of the tubes sealed in order to achieve sufficient internal pressure, providing air flow laterally to the absorbent (9). Humidification of the inlet air is provided using an evaporative pad matrix placed inside a rectangular shaped wick chamber (11). Air flow through the wick chamber is parallel to the evaporative pads, enabling moisture enhancement of the inlet air before entering the reaction chamber. An Xpleair (UK) XID series, inline duct fan (1) (d = 150 mm) is used to provide air flow and is connected to ducting (d = 100 mm) via a reducer. To eliminate thermal losses to the external environment, the complete system is insulated using 25 mm thick, foil lined glass wool. Temperature and relative humidity (RH) were recorded using the EK-H4 Eval Kit from Sensiron, AG, and Switzerland. Thermocouples (K type) with the maximum deviation of ±0.3°C for temperature and ±2% for relative humidity and air mass flow meter with the accuracy of ±2% were used for measuring the experimental data. Three sensor locations were used – (2) ambient, (3) manifold inlet and (4) reactor outlet.

2.2 Material selection

In previous work by the authors, a range of candidate nano-composite materials capable of producing adequate exothermic thermochemical reactions for 'open' THS when hydrated were investigated. A total of eight SIM (salt in matrix) composites were synthesized using the Insipient Wetness Technique (IWT) method and the materials were characterized.

V-$CaCl_2$ appeared to have excellent energy density, E_d coupled with good moisture uptake and response time to moisture uptake with TGA (Thermogravimetric analysis) also suggesting significant mass loss in the working range 30 < T < 140 ºC. These findings suggested that V-$CaCl_2$ appears to have very good potential for use in sorption jacket concept. Therefore it was selected as the sorption material to be experimented. Obtained scanning electron microscopy (SEM) images of raw vermiculite and $CaCl_2$ impregnated vermiculite were given in Figure 1. As seen in Figure 1a, the raw vermiculite has a lamellar structure with micro-porous channels (nominal $Ø_{pore}$ = 3.68μm) in between the lamellas

allowing large amount of salt to be impregnated. Figure 1b illustrates the lamellar structure of Vermiculite-$CaCl_2$. The SEM image of SIM-3a, obtained with 1000X magnification ratio shows the salt crystals loaded inside the horizontal nano-scale channels between the lamellas.

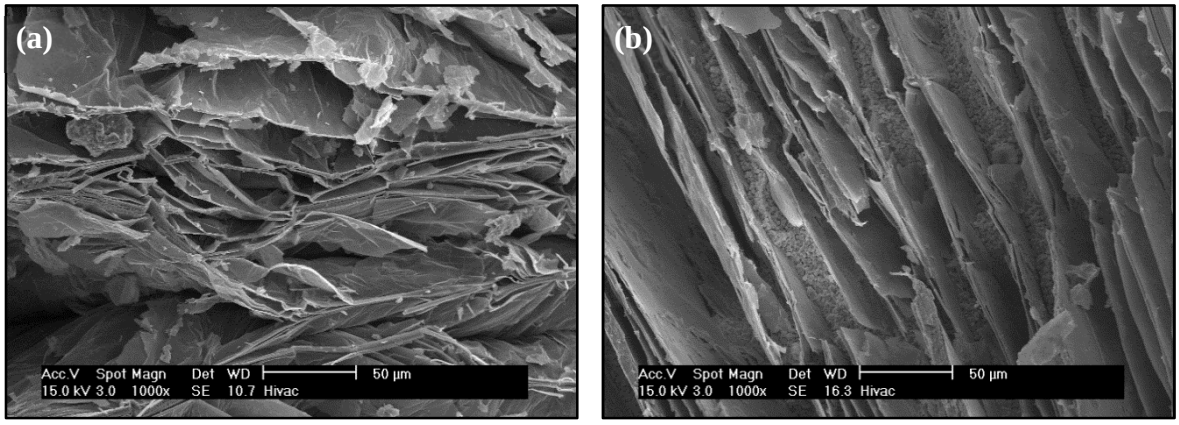

Figure 1 - SEM images of (a) Raw vermiculite, (b) SIM-3a

2. Results and discussion

Experimentally obtained V-CaCl2 performance is presented in Figure 3. To investigate the maximum thermal energy that can be extracted from Vermiculite-$CaCl_2$ in the developed testing rig, the cycle was allowed to run until the condition $T_{out} = T_{in} + 3$ °C were achieved (at the end of 20 hours for this case).

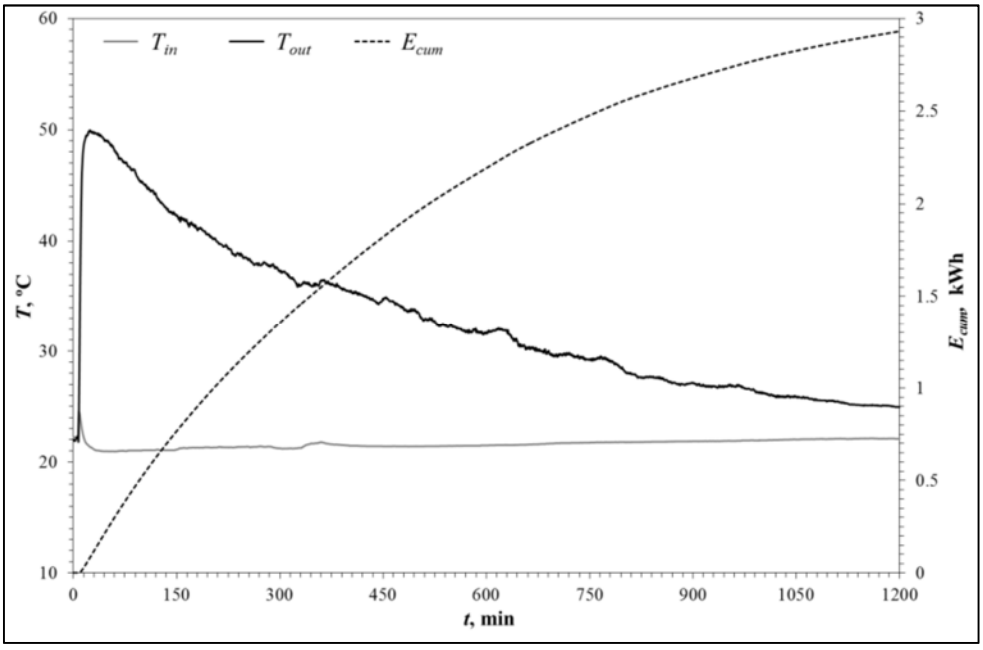

Figure 4.4.9 Thermal performance of SIM-3a over 1200 min. testing in Gen3 testing rig

During the test period the total thermal energy output reached 2.93 kWh with mass uptake of 1.41 g_{wv}/g_{abs}. It is interesting 2.93 kWh that was achieved only from 0.01 m^3 of storage volume, suggesting that THS has remarkable potential to be utilized in the proposed sorption jacket for reducing heat losses, increasing heat storage duration and reducing the extensive energy consumption in buildings for water heating.

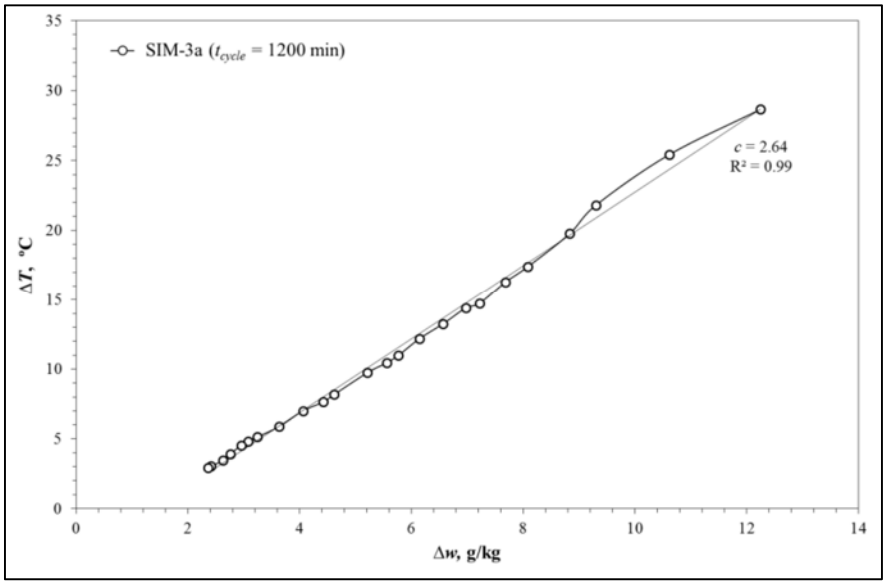

Figure 4.4.10 Correlation between Δw and ΔT for SIM-3a in the Gen3 rig

Figure 4.4.10 illustrates the correlation of Δw and ΔT over 20 hours testing of V-CaCl2. During the test period (t = 20 h), it can be observed that the correlation between Δw and ΔT is almost linear and independent of time. Recognizing and using this correlation will enable to design, operate and control the heat storage process with sorption jacket in an effective manner.

3. References

Chow, T. T., et al. (2010). "Modeling and application of direct-expansion solar-assisted heat pump for water heating in subtropical Hong Kong." Applied Energy 87(2): 643-649.

Freeman, T., et al. (1979). "Performance of combined solar-heat pump systems." Solar Energy 22(2): 125-135.

Greening, B. and A. Azapagic (2014). "Domestic solar thermal water heating: A sustainable option for the UK?" Renewable Energy 63: 23-36.

Greening, B. and A. Azapagic (2014). "Domestic solar thermal water heating: A sustainable option for the UK?" Renewable Energy 63(0): 23-36.

Huang, B. and J. Chyng (2001). "Performance characteristics of integral type solar-assisted heat pump." Solar Energy 71(6): 403-414.

Ito, S., et al. (1999). "Performance of a heat pump using direct expansion solar collectors." Solar Energy 65(3): 189-196.

Kong, X., et al. (2011). "Thermal performance analysis of a direct-expansion solar-assisted heat pump water heater." Energy 36(12): 6830-6838.

Kuang, Y., et al. (2003). "Study on a direct-expansion solar-assisted heat pump water heating system." International Journal of Energy Research 27(5): 531-548.

Kuang, Y. and R. Wang (2006). "Performance of a multi-functional direct-expansion solar assisted heat pump system." Solar Energy 80(7): 795-803.

Wile, D. (1935). "The measurement of expansion valve capacity." Refrigeration Engineering 8(1-8): 108-112.

Chow, T. T., et al. (2010). "Modeling and application of direct-expansion solar-assisted heat pump for water heating in subtropical Hong Kong." Applied Energy 87(2): 643-649.

Freeman, T., et al. (1979). "Performance of combined solar-heat pump systems." Solar Energy 22(2): 125-135.

Huang, B. and J. Chyng (2001). "Performance characteristics of integral type solar-assisted heat pump." Solar Energy 71(6): 403-414.

Ito, S., et al. (1999). "Performance of a heat pump using direct expansion solar collectors." Solar Energy 65(3): 189-196.

Kong, X., et al. (2011). "Thermal performance analysis of a direct-expansion solar-assisted heat pump water heater." Energy 36(12): 6830-6838.

Kuang, Y., et al. (2003). "Study on a direct-expansion solar-assisted heat pump water heating system." International Journal of Energy Research 27(5): 531-548.

Kuang, Y. and R. Wang (2006). "Performance of a multi-functional direct-expansion solar assisted heat pump system." Solar Energy 80(7): 795-803.

Wile, D. (1935). "The measurement of expansion valve capacity." Refrigeration Engineering 8(1-8): 108-112.